

## Ecological solar absorber coating: A proposal for the use of residual biomass and recycled materials for energy conversion

Luis Bernardo López-Sosa<sup>a,b</sup>, Mauricio González-Avilés<sup>b</sup>, Luis Mariano Hernández-Ramírez<sup>c</sup>, Ariosto Medina-Flores<sup>a</sup>, Tzarara López-Luke<sup>a</sup>, Mariela Bravo-Sánchez<sup>d</sup>, Juan Zárate-Medina<sup>a,\*</sup>

<sup>a</sup> Instituto de Investigación en Metalurgia y Materiales, Universidad Michoacana de San Nicolás de Hidalgo, Avenida Francisco. J. Mújica S/N Ciudad Universitaria, Morelia, Michoacán C.P. 58030, Mexico

<sup>b</sup> Posgrado en Ingeniería para la Sostenibilidad Energética, Universidad Intercultural Indígena de Michoacán, Carretera Pátzcuaro-Huecorio Km3, Pátzcuaro, Michoacán C. P. 61614, Mexico

<sup>c</sup> Facultad de Ciencias Físico-Matemáticas, Universidad Michoacana de San Nicolás de Hidalgo, Avenida Francisco. J. Mújica S/N Ciudad Universitaria, Morelia, Michoacán C.P. 58030, Mexico

<sup>d</sup> Centro Universitario de Ciencias Exactas e Ingeniería, Universidad de Guadalajara, Blvd. Marcelino García Barragán, 1421, C.P. 44430 Guadalajara, Jalisco, Mexico

### ARTICLE INFO

#### Keywords:

Ecological coating  
Solar absorber  
Thermosolar technology

### ABSTRACT

This paper discusses the development of a coating made of solid waste and residual biomass and its application as ecological solar absorber coating. This absorbent solar coating is made with a binder that consists of essential grapefruit rind oil and expanded polystyrene, both obtained from waste materials, as well as forest biomass soot (FBS) processed by mechanical grinding and used as a functional photothermal material. This mixture produces a paint that can be applied to metallic substrates to form a solar energy-absorbing surface. The characterization and evaluation is shown in three steps: (a) Characterization of the materials using XRD, SEM, TEM, XPS, Raman spectroscopy and IR; (b) coating evaluation using AFM, optical characterization to measure solar absorption, TG to determine the operating temperature and laser flash analysis to determine thermal conductivity; and (c) a testing with thermosolar technology to determine the thermal parameters of solar cookers. It has been identified that the pseudo-amorphous carbon in FBS has solar energy absorption capacity due to the  $sp^2$ - $sp^3$  bonds present in this kind of carbon, associated with the material's graphitic domain. Also, results show that the coating can be used with thermosolar technologies operating above 250 °C with a solar absorption index above 96%, and it has thermally-efficient properties. In addition, the coating, it shows better results with solar cookers than other coatings used with this technology, increasing cooking power, so it can potentially be employed with various thermosolar technologies due to the replicability of its materials, its low environmental impact and low economic cost.

### 1. Introduction

The research around Renewable Energy Sources (RES) has increased in recent years (Manzano-Agugliaro et al., 2013), mainly in the fields of bioenergy and solar energy. Currently, the exploitation of solar energy in the domestic sector includes the use of low-temperature thermal solar systems (80–150 °C), primarily to heat water and cook food (González-Avilés et al., 2017a, 2017b; Kalogirou, 2004). The operation and the performance of these systems depend strongly on the design and efficiency of the coatings since these factors allow a reduction on the fabrication and implementation costs and a low environmental impact (Altun-Çiftçioglu et al., 2016). Developing solar coatings entails considering that a material's light-absorbing capacity depends on its

electronic structure, the wavelength of the light, and surface smoothness (Feynman, 1985; Granqvist, 1991). Besides, when choosing the materials to be utilized, the main mechanisms of photoconversion must be considered (Atkinson et al., 2015; Gao et al., 2019; Kennedy, 2002): (a) plasmonic heating, (b) non-radiative semiconductor relaxation, and (c) thermal vibration of molecules. Some solar energy-absorbing paints made of organic materials allow photoconversion through molecular vibration, are generally low-cost, accessible, and simple to apply to solar collectors. They are ideal for low-power thermal solar systems that operate in low-to-medium temperature ranges ( $T < 300$  °C), and for applications in rural areas where acquiring more sophisticated materials may be difficult.

In the development of paints are involved 3 principal elements: (a) a

\* Corresponding author.

E-mail address: [जारate@umich.mx](mailto:जारate@umich.mx) (J. Zárate-Medina).

<https://doi.org/10.1016/j.solener.2020.03.102>

Received 30 December 2019; Received in revised form 25 March 2020; Accepted 27 March 2020

0038-092X/ © 2020 International Solar Energy Society. Published by Elsevier Ltd. All rights reserved.

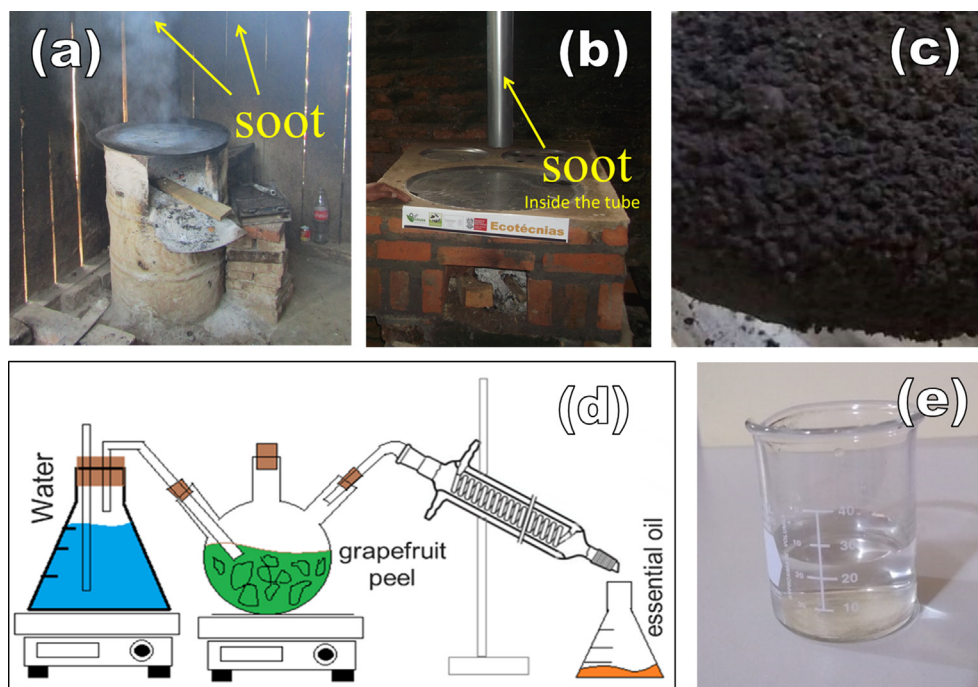


Fig. 1. (a) Traditional stove in a rural community kitchen where soot is accumulated in walls; (b) Patsari<sup>®</sup> stove duct where the soot is found; (c) soot particle agglomerates extracted from Patsari<sup>®</sup> stove duct; (d) steam drag to extract the essential grapefruit oil (e) essential grapefruit oil.

solvent; (b) a base or body; and (c) pigments. And in this work two materials derived from biomass are of special interest. On the one hand the of soot produced by the combustion of forest resources in Patsari<sup>®</sup> firewood-saving stoves (Fig. 1a–c) (Maserá et al., 2005). On the other hand, the grapefruit oil data from the citrus-producers' association in the citrus-growing region of the state of Michoacán, Mexico, indicate that around 30,000 tons of grapefruit are discarded annually. But grapefruit rind can be used to produce an organic solvent by extracting its essential oils, which contain diverse chemical compounds for this use (Arnoldo Bndoni, 2003; Nannapaneni et al., 2009), and this oil is low environmental impact. Most grapefruit oil –elaborated from rind– is made up of compounds of low molecular weight; that is, monoterpenoids, which represent over 70% by weight of this waste material (Pino and Sánchez, 2000; Soto et al., 2013). Monoterpenoids are volatile compounds with 10 carbon atoms and 2 units of isoprene that are thought to be one of the largest families of natural products (García et al., 2009; Grayson, 2000). Essential oils derived from citrus fruits contain the limonene terpenoid, which has been shown to act as a natural solvent of expanded polystyrene (Rivera et al., 2014), so it is a suitable solvent for our aim of producing a coating with low environmental impact.

The aim of this work is to develop a solar energy-absorbing paint coating that is efficient, low-cost and has a low environmental impact, generating a sustainable material. For this purpose, we complement previous research on Forest Biomass Soot (FBS), Fig. 1a–c, for applications in solar thermal technologies (Correa et al., 2014; López-Sosa et al., 2018). The FBS is material that functions as the absorption pigment in the solar spectrum. The binder suggested for use is derived from the essential oil of grapefruit rind, extracted by steam drag (Fig. 1d, e), which acts as the solvent. Finally, waste expanded polystyrene forms the base or body (Styrofoam) that dissolves easily in citrus oils. Here, both solvent and body have low environmental impact and exploit reusable waste and/or recycled materials. The result is an easy to make paint, which can be used in solar thermal technologies. The coating evaluation has been carried out using optical characterization to measure solar absorption, thermo-gravimetric tests to determine the maximum operating temperature of the coating, laser flash analysis to

determine thermal conductivity, and a surface morphology study.

## 2. Materials and methods

### 2.1. Characterization coating

The characterization of soot from forest biomass was performed with X-ray diffraction (XRD) using a D8 Advance Davinci model diffractor with Cu K $\alpha$  radiation (1.54056 Å). We also used scanning electron microscopy (SEM) with a Jeol JSM 7600F field-emission model; Transmission Electron Microscopy (TEM) with a field-emission Tecnai F-20 model; Raman spectroscopy with a Bruker Raman Senterra apparatus with a 532-nm laser, a power of 5mW, and a 50- $\mu$ m aperture; Infrared spectroscopy with a Bruker tensor 27 model (FTIR). And X-ray Photoelectron Spectroscopy (XPS) SPECS systems with an analyzer model Phoibos 150 (SPECS, Berlin); the system is equipped with a monochromatic Al K $\alpha$  x-ray source of 1486.7 eV photon energy which operates with a power of 300 W over a 3  $\times$  1 mm size spot; for charging compensation charge neutralization low energy electron beam was used; the survey spectrum was acquired at 40 eV of pass energy and step size of 0.5 eV, the high resolution spectrum values for the pass energy and the steps size were 15 eV and 0.1 eV, respectively. To deagglomerate soot particles, a planetary PM100 milling machine was used, with a velocity of 350 RPM (Suryanarayana, 2004). The Brunauer-Emmett-Teller (BET) method with a Quantasorb Jr device was used to measure the surface area before and after mechanical grinding.

The organic solvent used in this research was essential oil from grapefruit rind (*Citrus paradisi* L), while the body of the paint and ligand was polystyrene dissolved in the solvent, as a strategy for recycling expanded polystyrene. The suggested proportion of the mixture in mass was 3:1 of solvent and polystyrene, respectively (Rivera et al., 2014). The characterization of the grapefruit oil was performed by infrared spectroscopy, as specified previously. Evaluations of absorbent coatings (resulting paint = soot + binder) must be performed under both controlled laboratory conditions and in the field (outdoors) in order to corroborate experimental, laboratory results with the real performance of the coating. Both ways of testing were conducted in this

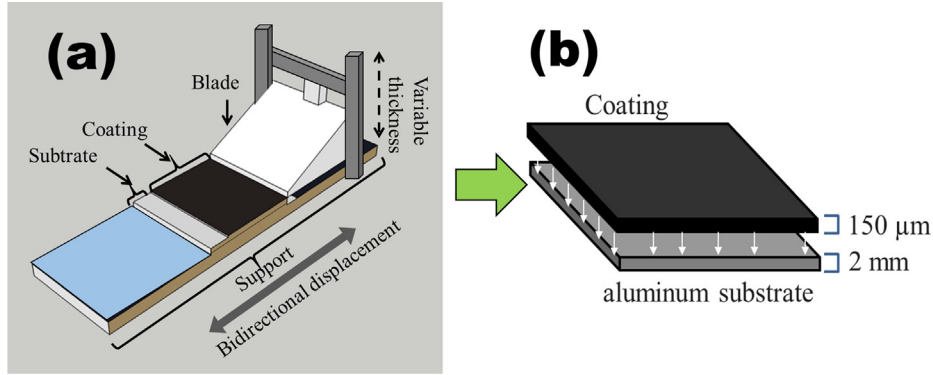


Fig. 2. (a) Coating application by flow-coating; (b) aluminum substrate with the proposed coating.

study. To homogenize the application of the paint on a metallic substrate (3003 aluminum alloy) it was necessary to use the flow-coating technique, (Mittal et al., 2010), (Fig. 2a); thus, the paint produced from the mixture of the binder and FBS was applied as a coating on the aluminum substrates (Fig. 2). The best photothermal properties for soot recurrences are obtained in the range of 100 to 200  $\mu\text{m}$  (Rebollo-Sandoval, 2017). Therefore, an average value for the size of the proposed coating has been defined.

The characterization of the coating developed considers: (a) surface morphology by Atomic Force Microscopy (AFM) and Scanning Electron Microscopy (SEM), as mentioned above; (b) chemical analysis utilizing infrared spectroscopy; and (c) thermal analysis. For this aspect, we estimated the coating's thermal conductivity at various temperatures, employing a Linseis LFA 1000 laser flash equipped with a NdYAG laser with a wavelength of 1064 nm, power of 1 mW and a pulse of 0.5 ms. Also, to evaluating the functionality of the coating and its stability to different temperatures required a Thermal Gravimetric Analysis (TGA) apparatus, Model-TGA500 (TA instruments) with an oxidizing atmosphere to simulate the outdoor conditions under which it would operate. Also, the absorbent surfaces developed (Fig. 2b) were evaluated comparatively in the field using a real solar irradiance test, as an indirect way of determining its solar absorption capacity (López-Sosa et al., 2018); (d) solar absorption: in this procedure, the spectra of hemispheric reflectance of the samples measured 0.3–2.5  $\mu\text{m}$  using a double-beam Perkin-Elmer Lambda 950 UV–VIS–NIR spectrophotometer equipped with a 150-mm integration sphere coated with Spectralon for diffuse reflectance. Solar absorbance ( $\alpha_s$ ) was calculated using the standard procedure (Farchado et al., 2018), an AM 1.5 between 0.3 and 2.5  $\mu\text{m}$ , and the following equation:

$$\alpha_s([0.3, 2.5], \theta_i, T_s) = \frac{\int_{0.3}^{2.5} [\alpha_\lambda(\lambda, \theta_i, T_s)] G_b d\lambda}{\int_{0.3}^{2.5} G_b d\lambda} \quad (1)$$

where  $\lambda$  is wavelength,  $\alpha_s(\lambda, \theta_i, T_s)$  is the spectral absorbance calculated from  $1 - \rho_\lambda(\lambda)$  with  $\rho_\lambda(\lambda)$  as the spectral hemispheric reflectance measured in the spectrophotometer, and  $G_b(\lambda)$  is the spectral solar irradiance.

The thermal emissivity of the coating,  $\varepsilon_T$ , was also determined using a Pekin Elmer Frontier FTIR spectrophotometer, with calculations from the hemispherical spectra of IR reflectance recorded from 2.5 to 17  $\mu\text{m}$  at room temperature, considering Kirchoff's law and the black body spectrum at 100  $^\circ\text{C}$  using the following equation (Duffie et al., 2003; López-Herraiz et al., 2017):

$$\varepsilon_T = \frac{\int_{2.5}^{17} [1 - \rho_\lambda] i_{\lambda,bb}(\lambda, T_s) d\lambda}{\int_{2.5}^{17} i_{\lambda,bb}(\lambda, T_s) d\lambda} \quad (2)$$

where  $\rho_\lambda$  is the spectral hemispherical reflectance measured in the spectrophotometer;  $i_{\lambda,bb}$  is the emission intensity of a black body for each wavelength at a given temperature.

## 2.2. Evaluation of the coating with a solar technology (solar cooker)

Having evaluated the solar absorbent paint, we assessed its performance with a solar cooking system, a Rural Solar Cooker (RSC) was used because it is a functional technology that is in used in diverse regions Mexico (González-Avilés et al., 2017a, 2017b). The coating was applied to a 5-liter pressure cooker that to evaluate the thermal parameters of the RSC. The main figure of merit specified in the ASAE S580 norm is standard cooking power (SCP) (Parker, 1980), which is calculated by multiplying the temperature difference,  $\Delta T = T_{\text{water}} - T_{\text{environment}}$  in 5 min by the mass of water ( $m$ ) in the pot and the specific heat of water ( $C_p = 4186 \text{ J/kgK}$ ), and then dividing the result by the elapsed time,  $\Delta\tau = 300 \text{ s}$ .

$$P_c = mc_p \frac{dT}{dt} \quad (3)$$

$P_c$  is cooking power,  $dT/dt$  is the differential of temperature with respect to time. To obtain the SCP, the cooking power was normalized to a value of 700  $\text{W/m}^2$  by the following equation.

$$P_s = P_c \left( \frac{700 \left( \frac{\text{W}}{\text{m}^2} \right)}{I} \right) \quad (4)$$

where  $I$  is average irradiance in the time interval ( $\text{W/m}^2$ ),  $P_c$  is the cooking power ( $\text{W}$ ),  $P_s$  is standard cooking power ( $\text{W}$ ). Results are shown by plotting  $P_s$  as a function of the difference between the temperature of the water and the ambient temperature at 50  $^\circ\text{C}$ . Another parameter evaluated during this procedure was yield (Thermal Operating performance), which was calculated with the following expression (Kundapur and Sudhir, 2009):

$$\eta = \frac{mC_p(T_{w2} - T_{w1})}{A \int I dt} \quad (5)$$

where  $m$  is the mass of water in the pot,  $T_{w2}$  is the final temperature of the water and  $T_{w1}$  is the initial temperature of the water,  $A$  is the area of solar collection,  $I$  is the irradiance and  $dt$  is the derived of time. Finally, we estimated heating time, which was calculated at 95% of the maximum temperature reached during the duration of the exposure test to solar radiation (González-Avilés et al., 2017a, 2017b).

## 3. Results and discussion

### 3.1. Materials and coating

Interest in soot from the combustion of organic materials has diversified in recent years (Kakunuri and Sharma, 2015; Singh et al., 2018; Xue et al., 2017). Studies of carbon nanoparticles from soot produced by combustion show that this is a multifunctional material. The results of the characterization of the FBS are described below. The

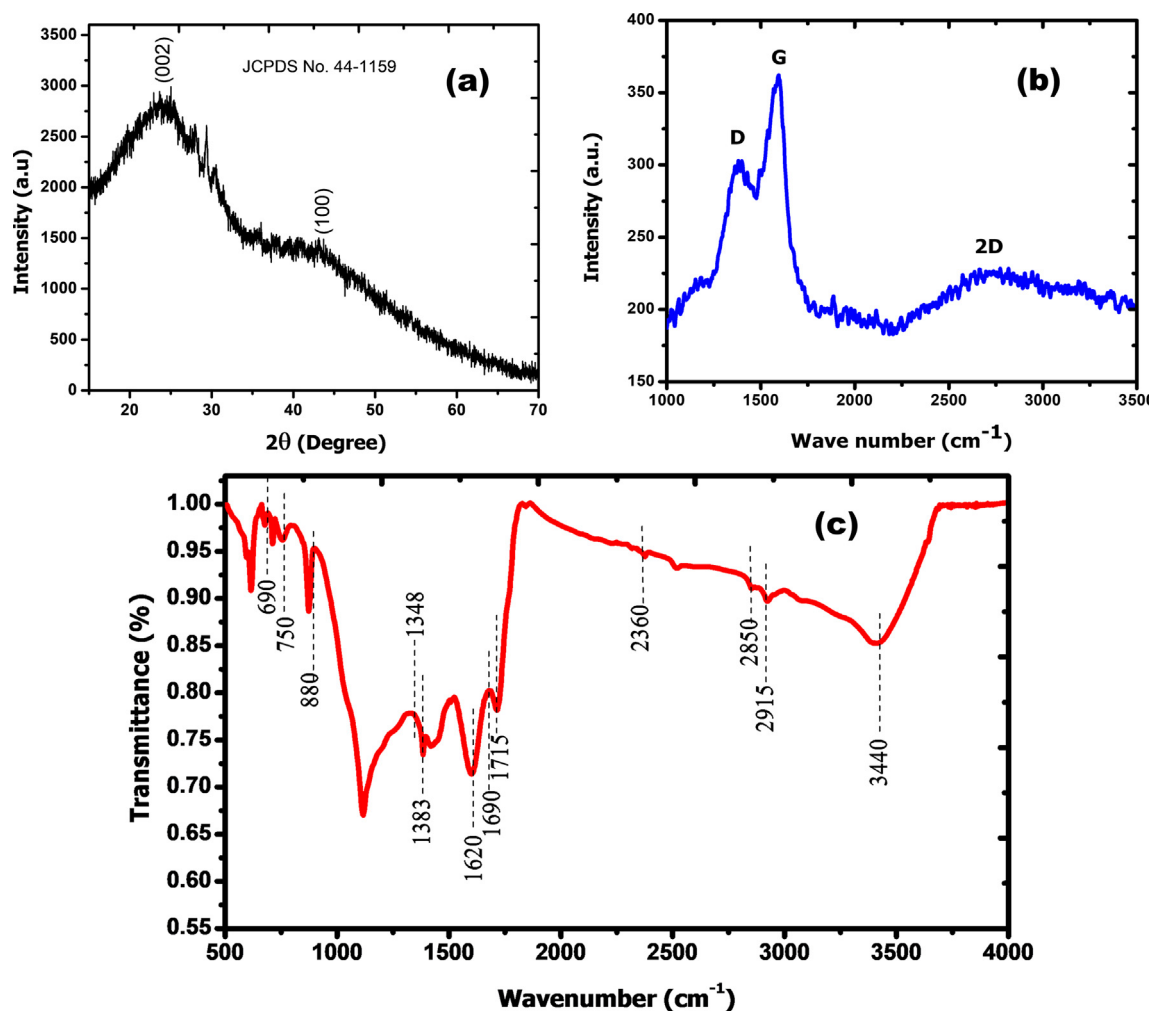


Fig. 3. Characterization of Forest Biomass Soot with (a) XRD, (b) Raman spectroscopy (c) FTIR spectroscopy.

XRD results show that this material presents pseudo-amorphous carbon and a certain crystalline phase, and that two diffraction peaks can be observed (Fig. 3a), which correspond to nanoparticulate carbon with graphitic crystalline traces at  $25.5^\circ$  and  $44^\circ$  (JCPDS No. 44-1159). These are largely amorphous and constitute honeycomb-type structures made of graphite-like carbon (Fig. 3a). This is consistent with others studies (Kakunuri & Sharma, 2015; Singh et al., 2018), which demonstrated the characterization of soot from combustion. The diffraction peaks reveal the presence of two planes (0 0 2) and (1 0 0) for the case of soot from combustion, a finding that also concurs with previous research (Kakunuri and Sharma, 2015; Singh et al., 2019; Xue et al., 2017).

The analysis of the FBS by Raman spectroscopy shows that it has three characteristic bands (Fig. 3b). Band D shows the amorphous or disordered graphite, while band G shows the first-order dispersion of the graphitic plane (crystalline); that is, the material's  $sp^2$  hybridized domain (Singh et al., 2019, 2018). Also evident is a third, weak and wide band at approximately  $2750\text{ cm}^{-1}$ , known as band 2D, which has been reported in others studies (Akhavan, 2015; Singh et al., 2019; Xie et al., 2017). This band is attributed to the appearance of a few layers of graphene in carbonaceous materials that can generate bands with higher values that correspond to multi-layer graphene. It is also interesting to determine whether the presence of this carbon allotrope contributes to the photothermal property of the FBS.

One of the main mechanisms of photoconversion that is best-known is thermal vibration in the molecules, which usually occurs in organic materials that absorb optical energy and transform it into heat. This is the case of many carbon allotropes (Gao et al., 2019), including carbon

and graphene nanotubes. In the present case, this is associated with pseudo-amorphous carbon. It is also well-known that this carbon allotrope contains  $sp^2$ - $sp^3$  bonds, as shown in some research (Bond and Bergstrom, 2006; Haerle et al., 2002); thus it is important to mention that the material's  $sp^2$  hybridized domain identified by Raman spectroscopy, made it possible to determine that the photothermal effect of the material is associated with this domain since,  $sp^2$ - $sp^3$  carbon allotropes have higher light absorption coefficients and greater efficiencies than other known light absorbers (Zhang et al., 2016). Therefore, the presence of pseudo-amorphous carbon helps produce the material's photothermal effect.

Another aspect of the FBS characterization is its chemical composition. This was analyzed by FTIR (Fig. 3c). The bands that appear at  $3440\text{ cm}^{-1}$  and  $1620\text{ cm}^{-1}$  are associated with the mode of stretching and flexion of the hydrogen bond in the hydroxyl group, and they suggest the presence of a phase of adsorbed water (Liang et al., 2014; Singh et al., 2018). Hence, the bands at  $2850\text{ cm}^{-1}$  and  $2915\text{ cm}^{-1}$  are attributed to the stretching of C–H (alkanes), and suggest that combustion was only partially-completed (Justin Raj et al., 2016). The band at  $2360\text{ cm}^{-1}$  represents a small amount of unburned organic material. In contrast, the bands at  $690\text{ cm}^{-1}$  and  $1590\text{ cm}^{-1}$  correspond to C–H functional groups of aromatic carbons; meanwhile, bands between  $1390\text{ cm}^{-1}$  and  $1750\text{ cm}^{-1}$  reveal the presence of proteins, lipids and fatty acids (Justin Raj et al., 2016; Singh et al., 2018), and those between  $750\text{ cm}^{-1}$  and  $900\text{ cm}^{-1}$  can be attributed to other compounds outside the plane of the CH aromatic band (Roden et al., 2006). Finally, the vibration band between  $1690\text{ cm}^{-1}$  and  $1715\text{ cm}^{-1}$

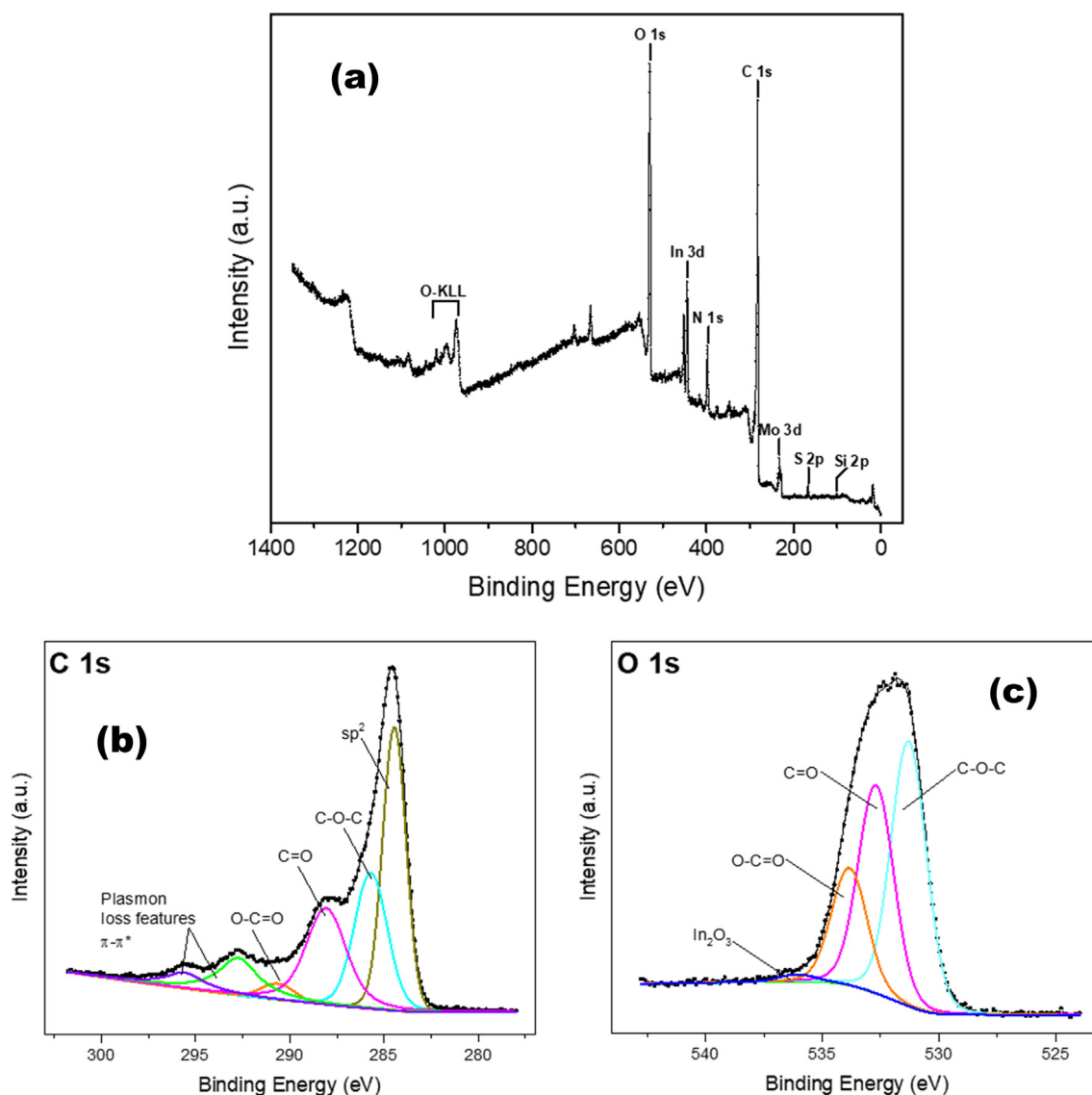


Fig. 4. XPS Characterization of Forest Biomass Soot: (a) Survey scan (b) high resolution spectra C1s (c) high resolution spectra O1s.

is linked to the stretching of the carboxyl group (Ess et al., 2016).

In summary, the FTIR spectrum shows a greater presence of primarily organic compounds, suggesting a favorable element for light absorption in these materials (Bond and Bergstrom, 2006). Complementary to this, the FTIR characterization supports the conjecture that the carbon present in the FBS is the element with photothermal properties, one that bodes well for the application of this material in solar thermoconversion systems. It is important to mention, in this regard, that previous research has shown that the presence of carbon in soot is quite large. Some research reported a carbon presence above 70% in FBS (Roden et al., 2006), a finding that concurs with the phase domain identified in the present study, as does the fact that the presence of a certain phase is associated with the material's absorption capacity.

The results of the XPS analysis are shown in Fig. 4. They are consistent with the Raman spectroscopy analysis in relation to the  $sp^2$ - $sp^3$  bonds, to which the solar absorption capacity is attributed. All these analyses show the results of  $sp^2$ - $sp^3$  bonds (Gaddam and Vander Wal, 2013).

Elemental quantification and chemical state analysis of the biomass sample was assessed from the XPS data and processed using AAnalyzer® software. The survey spectrum in Fig. 4a shows photoemission lines at

binding energies corresponding to oxygen, carbon, molybdenum, sulphur, silicon (Carabali et al., 2016), nitrogen and indium. The indium lines come from the substrate where the biomass sample was placed, and it was used as reference for shift correction being 1.98535 eV the shift value for correction of high-resolution spectra. The high-resolution spectra of the core levels C 1s (Fig. 4b), O 1s (Fig. 4c), and N 1s were analysed to identify the chemical species present in the FBS sample. In the case of C 1s were found 6 components. Among them, it is expected that two components come from a mixing of  $sp^2$  and  $sp^3$  hybridization, given the semi-amorphous nature of the FBS sample. It was found that the component at  $284.39 \pm 0.02$  eV is characteristic of the  $sp^2$  hybridization (C–C bond), and it is confirmed with the appearance of the  $\pi$ - $\pi^*$  plasmon loss features at  $292.72 \pm 0.03$  eV and  $295.55 \pm 0.04$  eV. Due the metallic nature of the  $sp^2$ , it is expected an asymmetry at the left side of the component peak, which was modelled using the double Lorentzian asymmetric line-shape together with the Voigt line-shape. The proper modelling of the asymmetry avoids including a not existent additional peak to cover the area corresponding to the tail at the left of the asymmetric peak. Although this component has characteristics of the  $sp^2$  hybridization (binding energy, asymmetry, loss features), the value of 1.38 for the FWHM is wider than the reported in the literature for pure  $sp^2$  (Susi et al., 2015). The analysis of

the subsequent components will give a complete picture to clarify the reason of it. All components in O 1s, N1s and C 1s were fitted using Voigt function excepting for  $sp^2$  as described previously. For background removal, a combination of Shirley-Sherwood and slope was used. The second component, which is at 1.29 eV from the  $sp^2$  peak, is characteristic of either  $sp^3$  or C–OH or C–O–C. To distinguish between them, the ratio of the concentration between the associated C–O components in the C 1s and the O 1s core levels, was calculated. We use sensitivity factors method to calculate concentration and even with less accuracy ( $\pm 10\%$  error) than the so-called first principles model, it gives a good insight regarding the concentration (Battistoni et al., 1985). The relationship between the concentration  $n_i$  for a component (i.e. chemical specie) in the element  $i$  and the area  $A_i$  of that component is given by  $n_i = A_i/S_i$ , where  $S_i$  the sensitivity factor for that element. From the core level O 1s, 5 peaks were identified qualitatively according to their binding energies located at  $531.29 \pm 0.02$  eV,  $532.69 \pm 0.05$  eV,  $533.82 \pm 0.04$  eV, and  $536.05 \pm 0.15$  eV, associated to C–O–C, C=O, O–C=O, and  $In_2O_3$ , respectively. The ratio concentration carbon/oxygen between the associated components were 1.95:1 for C–O–C, 2.5:1 for C=O and 1.1:2 for O–C=O. The ratio concentration between the component in In 3d at  $444.8 \pm 0.01$  eV and the component at  $536.05 \pm 0.15$  eV in O 1s is 2.3:3. This indium component acts as the reference instead the commonly used adventitious carbon since in this study the carbon is the element under study. According to the semiquantitative results, it was possible to confirm the existent of C–O–C and O–C=O, but two discrepancies were observed. The first is regarding the missing  $sp^3$  peak, which as mentioned above, it is expected to be present in the biomass sample at an average value of around 1.1 eV from  $sp^2$  according to the literature. Haerle et al. have reported a calculated and measured values of 1.0 and 0.9, respectively, for amorphous carbon (Haerle et al., 2002). It has been reported that the separation between the  $sp^2$  and  $sp^3$  peaks is in the range between 0.8 and 1.35 eV for amorphous carbon produced under different conditions (Wan and Komvopoulos, 2007). In this work, the separation between  $sp^2$  and the closest peak at high binding energy, is in the range mentioned but as the assessment of the ratio concentration indicates, that peak corresponds to C–O–C bond. By other side, the width of the Al-K $\alpha$  measured with Ag 3d with a pass energy of 15 eV is 1.1 eV, therefore components with a separation lower than this value are not possible to distinguish. This fact leaves only a range of 0.25 eV to incorporate a  $sp^3$  component. A feasible hypothesis considering a coaction of the factors: the width of the  $sp^2$  component, the resolution of the natural Al-K $\alpha$  x-ray line and the confirmation of the C:O ratio with the closest component to  $sp^2$  bond, suggest that the  $sp^2$  peak is the envelop of the  $sp^2$  and  $sp^3$  contributions as result of strong overlapping. The second discrepancy is regarding the third peak at  $288.06 \pm 0.07$  and  $532.69 \pm 0.05$  assigned to C=O in C 1s and O 1s, respectively, the C:O concentration ratio is 2.4:1, which is far from the expected value. A contribution of chemical bonding between carbon and nitrogen atoms must be present in this case resulting in an additional contribution to the area of the peak at  $288.06 \pm 0.07$  eV. This assumption is under the consideration that the principal contribution to the total area of nitrogen; pyrrolic-N is in the range between 285.5 and 288.3 eV in C 1s and 398.9–400.9 eV in N 1s (Susi et al., 2015), which agrees with the results as indicated in Table A.1. Continuing with the peak at  $290.61 \pm 0.18$ , its assignation to O–C=O is strongly supported with the C:O ratio concentration calculated with the area of the O 1s component at  $533.82 \pm 0.04$ , which is 1.06:2. The last two peaks at  $292.72 \pm 0.03$  eV and  $295.55 \pm 0.04$  eV are plasmon loss features related with delocalized  $\pi$  electrons in  $sp^2$  hybridization.

Transmission electron microscopy (TEM) allowed us to obtain more precise data on the nanometric size of the FBS particles (Fig. 5a). The agglomerates of nanometric order contain particles whose size is < 100 nm. This determination concurs with previous research (Carabali et al., 2016; Martins et al., 1998). Moreover, the TEM images confirmed the existence of a nano-chain structure of carbon nanoparticles with a

mean diameter < 100 nm. The tendency of the carbon nanoparticles to form chains—as can be seen in Fig. 4a—can be attributed to their strong union and/or adhesion (Singh et al., 2018). The TEM analysis also made it possible to observe the amorphous part of the material, short-range, nano-sized carbon structures (Fig. 5b), and the presence of graphitic structures with dislocations that show deformation in the short-range crystalline network. Thus, we confirmed the presence of the graphite plane (0 0 2) that was revealed by DRX. This matches with the studies for soot of combustion (López-Sosa et al., 2019a, 2019b; Singh et al., 2019; Su et al., 2011), that show a TEM characterization. It also concurs, complementarily, with the characterization described above. According to these results, the functional SFB is interesting for possible applications as a solar energy-absorbing material in coatings. These applications are described in the next section.

The binder proposed for the coating in the present research consists of a solvent based on essential grapefruit oil, and a base (body) of expanded polystyrene which is easily-dissolved (García et al., 2009), due to the high presence of limonene-type terpenoids (Pino and Sánchez, 2000; Schulz et al., 2002). For this reason, the FTIR analysis evidenced the bands at  $886\text{ cm}^{-1}$ ,  $1436\text{ cm}^{-1}$ ,  $1453\text{ cm}^{-1}$  and  $1644\text{ cm}^{-1}$ , which are associated with the limonene terpenoids present in the oil analyzed (Kalasinsky and McDonald, 1983) (Fig. 6a). To complement this analysis, we used Raman spectroscopy. It is important to point out that some studies (Partal Ureña et al., 2009; Pino and Sánchez, 2000; Seidler-Lozykowska et al., 2010), show the characteristic bands of limonene terpenoids, which can also be observed in Fig. 6b. Regarding limonene, signals can be recognized near  $1645\text{ cm}^{-1}$  due to the presence of alkenes (C=C ethylene type, and cyclohexene). A strong vibration of the deformation of the ring between  $740$  and  $760\text{ cm}^{-1}$  (Schulz and Baranska, 2007; Seidler-Lozykowska et al., 2010) is also observable. Both characterizations (FTIR, Raman) confirm the presence of the limonene terpenoid; that is, the compound responsible for solubilizing the expanded polystyrene. The polystyrene utilized presents a characteristic FTIR spectrum that is associated with the  $2850\text{ cm}^{-1}$ ,  $2930\text{ cm}^{-1}$ ,  $3000\text{ cm}^{-1}$ , (Jabbari & Peppas, 1993),  $3030\text{ cm}^{-1}$ ,  $3060\text{ cm}^{-1}$ ,  $3085\text{ cm}^{-1}$  and  $3105\text{ cm}^{-1}$  bands (Jabbari and Peppas, 1993; Liang and Krimm, 1958). Fig. 6a shows an integrated image of the bands characteristic of the essential oil, the FBS and the expanded polystyrene.

The weight concentration in the paint was 60% binder/40% soot (Fig. 6a–d) (López-Sosa et al., 2018). The FBS was ground mechanically and then mixed in to produce the paint. Grinding helps to disaggregate and break up the chains of carbon nanoparticles and achieve an estimated increase of the surface area from  $50.55$  to  $70.23\text{ m}^2/\text{g}$  (Fig. 7). A macroscopic view shows a finer appearance and less dense soot.

SEM analysis allowed us to corroborate that FBS is a nanometric material that form large aggregates before grinding (Fig. 7a), because of the time of collection from the firewood-saving stoves. After grinding, the agglomerates of nanometric particles were smaller, and it was possible to visualize the soot particles (Fig. 7b).

When the ground soot was utilized, the surface obtained upon applying the coating on the metallic substrates was more homogeneous and had—qualitatively—greater adhesion (Fig. 7d, f). In contrast, the unground FBS produced much more irregular coatings (Fig. 7c, e) that caused the paint to easily detach from the metallic substrates. Mechanical grinding, therefore, produced a greater contact area for the material by increasing the surface area, thus generating more homogeneous surfaces.

The coating's solar absorption is acceptable, as shown by the reflectance curve (Fig. 8a). In fact, when compared to other, low-cost coatings (Farchado et al., 2018; Katumba et al., 2005), our mixture showed high values for solar absorption. To estimate solar absorption, we used the equation (1):  $\alpha_s = 0.968$ . This is, actually, one of the highest values reported in the literature on recently-developed, low-cost coatings (Gao et al., 2017; Prasad et al., 2018). The emissivity of the proposed coating was  $\varepsilon_T = 0.924$ . The selectivity of the material

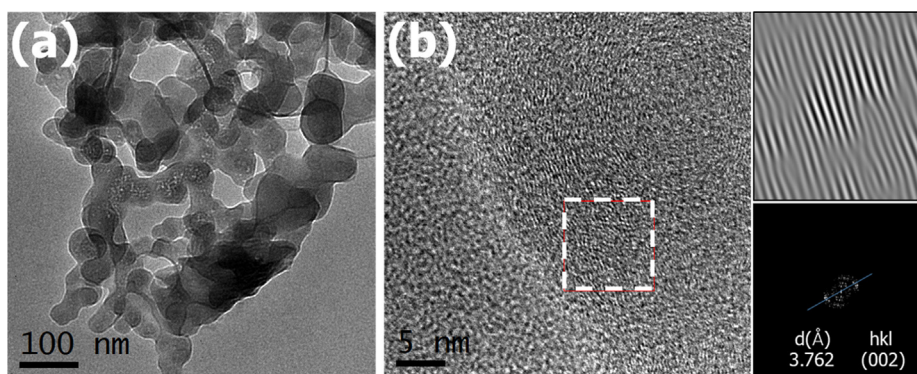


Fig. 5. TEM micrographs of soot from forest biomass (a) Bright field; (b) HRTEM and filtered area with its correspond diffraction pattern.

( $\alpha_s/\varepsilon_T$ ) is 1.04. In low cost coatings for solar cookers these values are acceptable (González-Avilés et al., 2019; Servín et al., 2016), in addition, it is important to highlight the low environmental impact that this material has.

Fig. 8b shows the results for the parameter of thermal conductivity of the coating at different temperatures. Previous studies involving SBF have hypothesized a relation between thermal conductivity and temperature increase; however, they fail to show any explicit relation between conductivity and useful heat transfer in end-use apparatuses. In this case, the results shown in Fig. 8b are distinct from those with some researches (Wamae et al., 2018), because in this study the photothermal property of the material, soot, caused conductivity to increase as the temperature was increased. In fact, at temperatures above 100 °C, the material experienced a significant increase of thermal conductivity, indicating that the amount of heat transferred is greater, and that this occurs faster at higher temperatures. Fig. 8c illustrates that, as the solar energy hits the surface of the coating, the photothermal effect generates heat transfer towards the metallic substrate. The greater the thermal

conductivity, the greater the amount of useful accumulated heat; this is an ideal situation for coatings used in low-power, thermal solar technologies, especially because they operate in the range of 100–200 °C, and the useful heat translates into the efficiency with which these technologies perform thermal tasks; for example, dehydrating or cooking foods, and heating or distilling water.

Regarding the issue of material degradation at different temperatures, TGA results are shown with respect to a temperature ramp that reaches 400 °C. Clearly, the coating begins to degrade at around 300 °C (Fig. 8d), due to the presence of the binder, for it is reported that the functional material begins to degrade at a temperature above 400 °C (Kennedy, 2002). These results are encouraging because a variety of thermosolar systems operate at temperatures around 200 °C, which would allow an optimum use of the coating developed in here that, furthermore, is ecological.

The coating was also evaluated outdoors using an experimental protocol in which all the coatings analyzed on the metallic substrates were exposed to real solar radiation to record the maximum

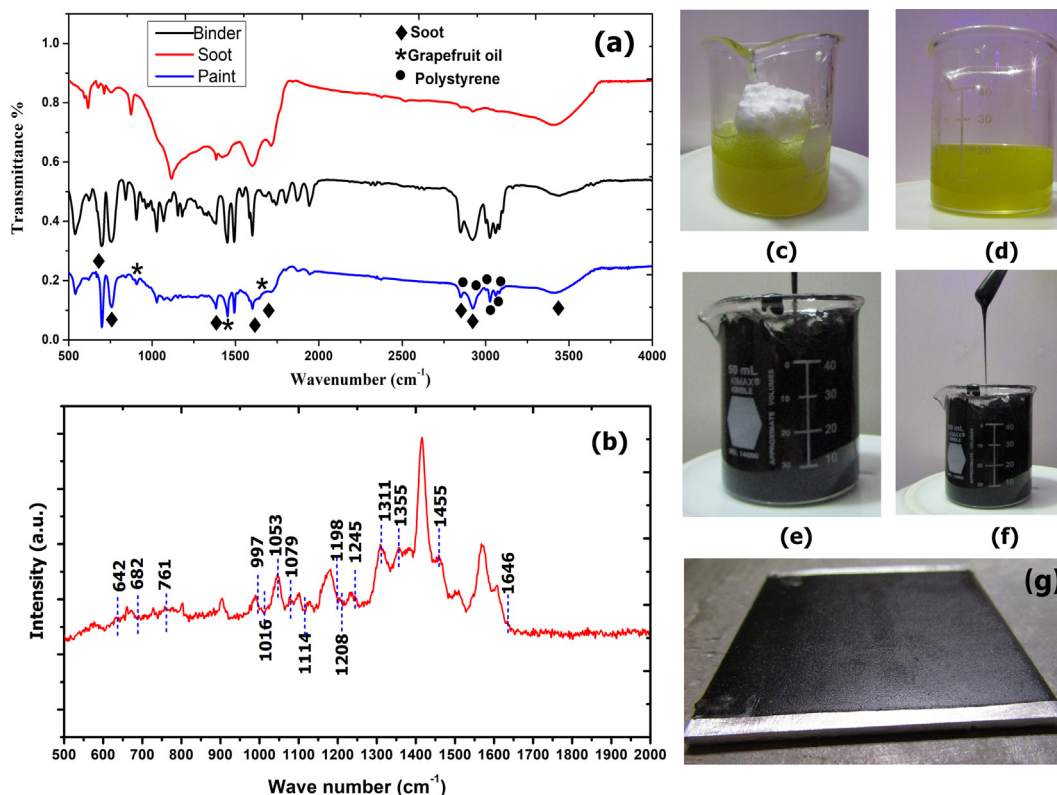


Fig. 6. (a) FTIR solar absorbent proposed coating; (b) Raman grapefruit oil; (c) essential grapefruit oil; (d) binder with dissolved oil and polystyrene; (e) incorporation of soot and binder; (f) homogeneous paint; (g) coating on metal substrate.

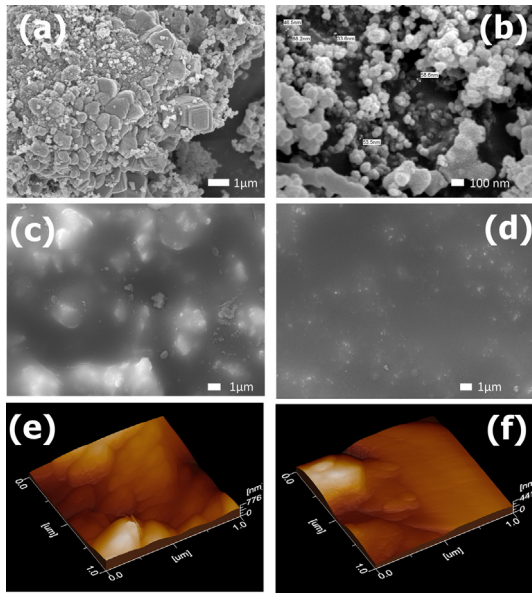


Fig. 7. SEM of: (a) agglomerates of non-ground SFB; (b) SFB after grinding; (c) coating surface of unground SFB; (d) coating surface of ground SFB. AFM: (e) coating surface of unground SFB; (f) coating surface of ground SFB.

temperature that the substrate reached. This is an indirect way of measuring the coating’s functionality and determining the velocity of heating, or heat transfer (López-Sosa et al., 2018). The surfaces to be tested were placed in a thermally-insulated box with a glass cover to minimize loss during heat transfer (Fig. 8e). We measured the maximum temperature of the metallic substrate. Results are shown in Fig. 8f, where it is clear that the coating’s functionality contrasts with the estimated properties of high solar absorption.

### 3.2. Evaluation of the coating in solar cooker.

To corroborate the coating’s functionality, we used an aluminum pot to evaluate a real solar cooking system (Fig. 9a). The paint was applied to the pot without difficulty, just like any conventional paint (Fig. 9b). The pot employed is part of the solar stove in which the coatings’ cooking performance was assessed. The thickness range is mostly between 100 and 200 μm, which is the best range for photo-thermal properties (Fig. 9c). The results of the coatings in relation to cooking power are shown in Fig. 9d.

The results presented in Fig. 9d show that the coating developed in this work generated high cooking power and improved the characteristics of the thermal values reported for this technology compared to other coatings (Sosa et al., 2014). The results for thermal yield and heating, the cooking times, and the optical properties are shown in Table 1.

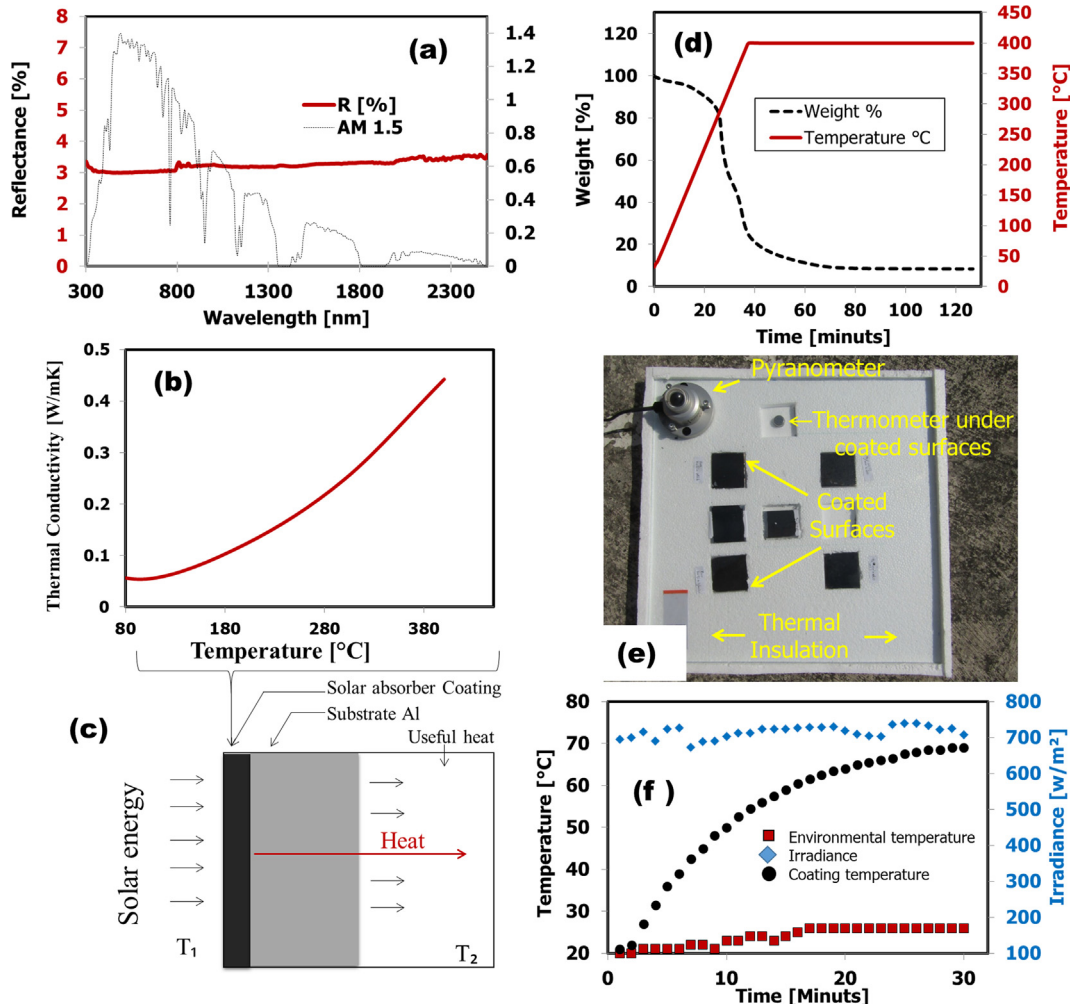
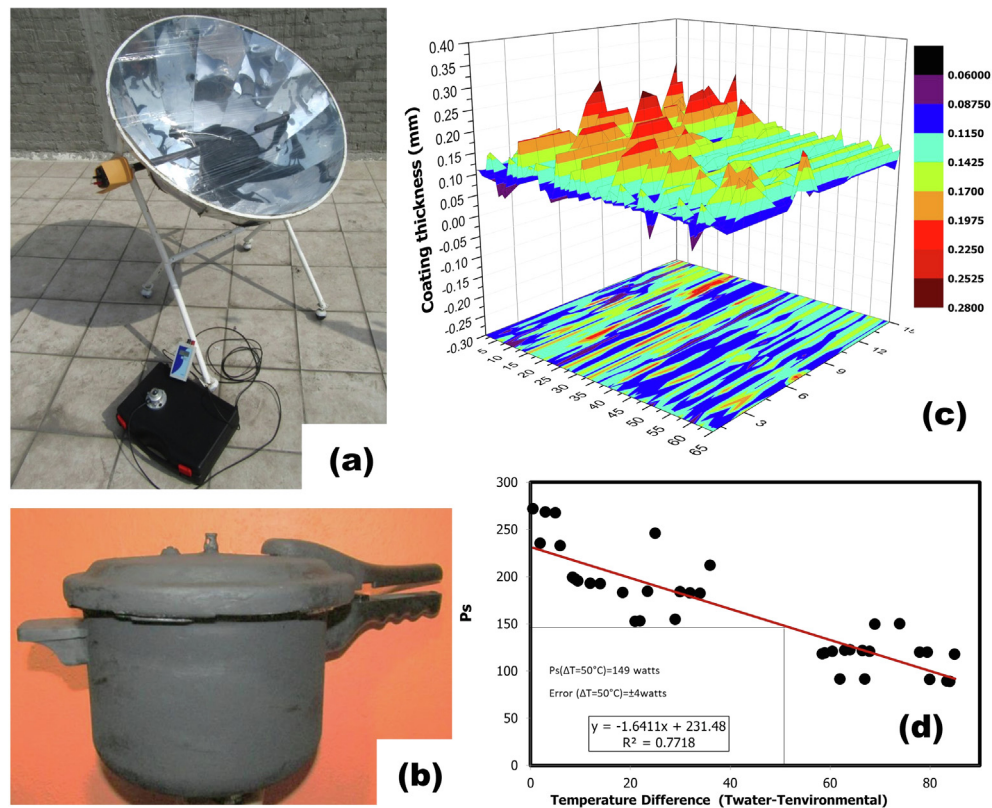


Fig. 8. (a) Optical analysis of the proposed coating; (b) analysis of thermal conductivity; (c) diagram of the heat transfer associated with thermal conductivity; (d) TGA analysis at 400° C; (e) experimental arrangement of the coating with solar radiation; (f) test with solar radiation.



**Fig. 9.** (a) Rural solar cooker (RSC), (b) aluminum pot with proposed coating, (c) projection of the thickness of the coating on the pot as a surface plot and (d) analysis of standard cooking power.

**Table 1**  
Results of the thermal parameters of the proposed coating applied to the RSC.

Thermal parameter	Soot coating
Cooking power	149 Watts
Heating time	83 min
Thermal yield	45%
Solar absorption	0.968

### 3.3. Discussion and final remarks

The present coating is competitive, because it is simple to make, easy to apply as a paint, it is low cost and low environmental impact, compared to other coatings for solar cookers (Cuce and Cuce, 2013; Herez et al., 2018). In regards to the thermal parameters evaluated, the values recorded were better than those reported with the use of other low-cost coatings (Sosa et al., 2014). The coating developed it is an ecological product with low environmental impact when compared to other coatings used in thermosolar applications, as it can be seen in various the environmental impact analysis (Altun-Çiftçioğlu et al., 2016; Gökulu et al., 2011; Lamnatou and Chemisana, 2017; Sánchez-Cruces et al., 2014).

Research previous on environmental impact for solar coating absorber (Altun-Çiftçioğlu et al., 2016), shows the process used to obtain a solar absorbent surface of  $1 \text{ m}^2$  of coating (as a comparative functional unit). Among the diverse materials used to fabricate that coating we find nickel, acid hydrogen sulfide, sodium carbonate, sodium hydroxide and water, all in diverse proportions. Their study showed that obtaining the functional unit of solar coating required 6.55 MJ of electrical energy, while treating the metallic surface to which the coating would be applied demanded another 4.678 MJ. In contrast, in this work, the process of obtaining the soot-based coating consumed only 2.160 MJ of

electrical energy; that is, < 20% of the net energy compared to the coating reported by Altun (Altun-Çiftçioğlu et al., 2016) (in both cases, this considers only the process of integrating the materials utilized). This was the only energy consumed during the process of obtaining the essential oil. If this process were performed using solar concentration –which is perfectly feasible– then the consumption of electrical energy would be null, and minor environmental impact.

The production cost of a liter of the developed paint is approximately 1 dollar (USD); that represents only the cost of the electrical energy requirement (30 kWh/l; and \$0.033USD/kWh in Mexico), because the materials used are solid waste with no economic value in Mexico at this time; in addition, in many cases those who generate this waste pay for the collection. Also, this paint is easy to make and apply in solar thermal technologies.

In functional terms, we developed a new coating that represents a useful option for thermosolar technologies. This type of coating will be very useful in situations that report the implementation of thermosolar technologies in the rural sector (González-Avilés et al., 2017a, 2017b; López-Sosa et al., 2019a, 2019b), because it allows the replicability and maintenance of the technologies implemented and reduces the costs of the materials involved.

### 4. Conclusions

Forest Biomass Soot (FBS) is a useful photothermal material for applications with solar energy absorbers. As biomass residue, it is a low-cost material with low environmental impact. This material presents large amounts of amorphous carbon and a certain presence of crystalline traces with a graphitic domain. This material's absorption capacity and thermal conductivity show the high efficiency of the coating for applications with thermosolar technologies. Based on the characterization techniques employed, it is important to note that the pseudo-amorphous carbon in FBS has solar energy absorption capacity due to

the sp<sup>2</sup>-sp<sup>3</sup> bonds present in this kind of carbon, associated with the material's graphitic domain, as determined by Raman spectroscopy and XPS analysis. This represents an additional line of research for future work. One of the most important results of this research is the proposal for a new solar energy-absorbing coating made of waste and recycled materials, like expanded polystyrene. The application of the proposed coating in a solar cooker increases the thermal efficiency by 10% and the cooking power by 19 W, more than a conventional black paint; demonstrating a better performance in this technology. This coating offers an ecological alternative that fosters the use of ecomaterials, is of low cost, and is easily-replicated, so it can easily be incorporated into thermosolar technologies used in the rural sector, where it is not always possible to obtain sophisticated materials. The binder developed is a complementary ecological option for producing a new solar energy-absorbing coating, since it is made of low-cost biomass residues and recycled materials that do not affect the photothermal capacity of the functional material (FBS) and are easy to replicate. In future research, we will analyze the life-cycle of the material to determine its precise environmental impact and compare this to existing coatings. Finally, we have demonstrated that the coating proposed is useful for solar thermal technologies, so its application in other thermosolar technologies can be foreseen.

### Declaration of Competing Interest

The authors declare that they have no known competing financial interests or personal relationships that could have appeared to influence the work reported in this paper.

### Acknowledgements

The authors thank the Departamento de Térmica y Fluidos, Universidad Carlos III de Madrid, Dr. Ángel Morales Sabio from the Centro de Investigaciones Energéticas, Medioambientales y Tecnológicas de Madrid, Spain, for their technical assistance; CIC-Universidad Michoacana de San Nicolás de Hidalgo, Mexico's Consejo Nacional de Ciencia y Tecnología (CB—287852 CONACyT and CONACyT-247719), 2019 UC-MEXUS-CONACyT, Mexico; and the indigenous communities in the state of Michoacán, Mexico, for their support in the development of this research.

### Appendix A. Supplementary material

Supplementary data to this article can be found online at <https://doi.org/10.1016/j.solener.2020.03.102>.

### References

- Akhavan, O., 2015. Bacteriorhodopsin as a superior substitute for hydrazine in chemical reduction of single-layer graphene oxide sheets. *Carbon N. Y.* 81, 158–166. <https://doi.org/10.1016/j.carbon.2014.09.044>.
- Altun-Çiftçioglu, G.A., Gökulu, O., Kadirgan, F., Kadirgan, M.A.N., 2016. Life cycle assessment (LCA) of a solar selective surface produced by continuous process and solar flat collectors. *Sol. Energy* 135, 284–290. <https://doi.org/10.1016/j.solener.2016.05.049>.
- Arnoldo Bndoni, 2003. Los Recursos Vegetales Aromáticos en Latinoamérica Cytad Ciencia Y Tecnologia Para El Desarrollo.
- Atkinson, C., Sansom, C.L., Almond, H.J., Shaw, C.P., 2015. Coatings for concentrating solar systems - a review. *Renew. Sustain. Energy Rev.* 45, 113–122. <https://doi.org/10.1016/j.rser.2015.01.015>.
- Battistoni, C., Mattogno, G., Paparazzo, E., 1985. Quantitative surface analysis by XPS: a comparison among different quantitative approaches. *Surf. Interface Anal.* 7, 117–121. <https://doi.org/10.1002/sia.740070303>.
- Bond, T.C., Bergstrom, R.W., 2006. Light absorption by carbonaceous particles: an investigative review. *Aerosol Sci. Technol.* 40, 27–67. <https://doi.org/10.1080/02786820500421521>.
- Carabali, G., Castro, T., De La Cruz, W., Peralta, O., Varela, A., Amelines, O., Rivera, M., Ruiz-Suarez, G., Torres-Jardón, R., Martínez-Quiroz, E., Policrionades, R., Murillo, G., Moreno, E., Muñoz-Muñoz, F., Molina, L., 2016. Morphological and chemical characterization of soot emitted during flaming combustion stage of native-wood species used for cooking process in western Mexico. *J. Aerosol Sci.* 95, 1–14. <https://doi.org/10.1016/j.jaerosci.2016.01.008>.

- Cuce, E., Cuce, P., 2013. Theoretical investigation of hot box solar cookers having conventional and finned absorber plates. *International Journal of Low-Carbon Technologies* 10 (3), 238–245. <https://doi.org/10.1093/ijlct/ctt052>. In this issue.
- Correa, F., Gonzalez, M., Servin, H., Marquez, F., Rutiaga, J.G., Lemus, A.A., Reguerad, E., Alonso, V., 2014. Development of a selective low cost absorbing surface based on soot for solar thermal applications. *Energy Procedia* 57, 1565–1572. <https://doi.org/10.1016/j.egypro.2014.10.148>.
- Duffie, J.A., Beckman, W.A., Worek, W.M., 2003. *Solar Engineering of Thermal Processes*, fourth ed. *Journal of Solar Energy Engineering*. <https://doi.org/10.1115/1.2930068>.
- Ess, M.N., Ferry, D., Kireeva, E.D., Niessner, R., Ouf, F.X., Ivleva, N.P., 2016. In situ Raman microspectroscopic analysis of soot samples with different organic carbon content: Structural changes during heating. *Carbon N. Y.* 105, 572–585. <https://doi.org/10.1016/j.carbon.2016.04.056>.
- Farchado, M., Rodríguez, J.M., San Vicente, G., Germán, N., Morales, A., 2018. Optical parameters of a novel competitive selective absorber for low temperature solar thermal applications. *Sol. Energy Mater. Sol. Cells* 178, 234–239. <https://doi.org/10.1016/j.solmat.2018.01.031>.
- Feynman, R.P., 1985. *The Strange Theory of Light and Matter*, second ed. Princeton University Press, Princeton.
- Gaddam, C.K., Vander Wal, R.L., 2013. Physical and chemical characterization of SIDI engine particulates. *Combust. Flame* 160, 2517–2528. <https://doi.org/10.1016/j.combustflame.2013.05.025>.
- Gao, M., Zhu, L., Peh, C.K., Ho, G.W., 2019. Solar absorber material and system designs for photothermal water vaporization towards clean water and energy production. *Energy Environ. Sci.* 12, 841–864. <https://doi.org/10.1039/c8ee01146j>.
- Gao, X.H., Guo, Z.M., Geng, Q.F., Ma, P.J., Liu, G., 2017. Microstructure and optical properties of SS/Mo/Al<sub>2</sub>O<sub>3</sub> spectrally selective solar absorber coating. *J. Mater. Eng. Perform.* 26, 161–167. <https://doi.org/10.1007/s11665-016-2445-1>.
- García, M.T., Gracia, I., Duque, G., de Lucas, A., Rodríguez, J.F., 2009. Study of the solubility and stability of polystyrene wastes in a dissolution recycling process. *Waste Manag.* 29, 1814–1818. <https://doi.org/10.1016/j.wasman.2009.01.001>.
- Gökulu, O.G., Altun-Çiftçioglu, G.A., Kadirgan, M.A.N., 2011. Cradle to gate life cycle assessment of continuous production for solar collector selective surface. *Fen Bilimleri Dergisi* 23 (4), 160–170.
- González-Avilés, Mauricio, González-Avilés, José Juan, Servín-Campuzano, H., 2019. Thermal model of a solar concentration cooker: a parameter variation study to estimate thermal properties. *Rev. Int. Métodos Numéricos para Cálculo y Diseño en Ing.* 35.
- González-Avilés, Mauricio, Bernardo López-Sosa, L., Servín Campuzano, H., 2017a. Evaluation framework for small-dimension solar cookers Cómo citar: Marco de evaluación para cocinas solares de pequeña dimensión. *Acta Univ.* 27, 69–75. <https://doi.org/10.15174/au.2017.1214>.
- González-Avilés, M., López-Sosa, L.B., Servín-Campuzano, H., González-Pérez, D., 2017b. Adopción tecnológica sustentable de cocinas solares en comunidades indígenas y rurales de michoacán. *Rev. Mex. Ing. Quim.* 16, 271–280.
- Granqvist, C.G., 1991. Solar energy materials - overview and some examples. *Appl. Phys. A Solids Surfaces* 52, 83–93. <https://doi.org/10.1007/BF00323721>.
- Grayson, D.H., 2000. Monoterpenoids. *Nat. Prod. Rep.* 17, 385–419. <https://doi.org/10.1039/a804437f>.
- Haerle, R., Riedo, E., Pasquarello, A., Baldereschi, A., 2002. (formula presented) hybridization ratio in amorphous carbon from C (formula presented) core-level shifts: X-ray photoelectron spectroscopy and first-principles calculation. *Phys. Rev. B - Condens. Matter Mater. Phys.* 65, 1–9. <https://doi.org/10.1103/PhysRevB.65.045101>.
- Herez, Amal, Ramadan, Mohamad, Khaled, Mahmoud, 2018. Review on solar cooker systems: Economic and environmental study for different Lebanese scenarios. *Renewable and Sustainable Energy Reviews* 81, 421–432. <https://doi.org/10.1016/j.rser.2017.08.021>. In this issue.
- Jabbari, E., Peppas, N.A., 1993. Use of ATR-FTIR to study interdiffusion in polystyrene and poly(vinyl methyl ether). *Macromolecules* 26, 2175–2186. <https://doi.org/10.1021/ma00061a006>.
- Justin Raj, C., Kim, B.C., Cho, B.B., Cho, W.J., Kim, S.J., Park, S.Y., Yu, K.H., 2016. Electrochemical supercapacitor behaviour of functionalized candle flame carbon soot. *Bull. Mater. Sci.* 39, 241–248. <https://doi.org/10.1007/s12034-015-1113-7>.
- Kakunuri, M., Sharma, C.S., 2015. Candle soot derived fractal-like carbon nanoparticles network as high-rate lithium ion battery anode material. *Electrochim. Acta* 180, 353–359. <https://doi.org/10.1016/j.electacta.2015.08.124>.
- Kalasinysky, V.F., McDonald, J.T., 1983. GC/FTIR Spectra of Terpenes 21, 193–200.
- Kalorigou, S.A., 2004. Solar thermal collectors and applications. *Progr. Energy Combust. Sci.* <https://doi.org/10.1016/j.pecs.2004.02.001>.
- Katumba, G., Lu, J., Olumekor, L., Westin, G., Wäckelgård, E., 2005. Low cost selective solar absorber coatings: Characteristics of carbon-in-silica synthesized with sol-gel technique. *J. Sol-Gel Sci. Technol.* <https://doi.org/10.1007/s10971-005-4793-4>.
- Kennedy, C.E., 2002. Review of Mid- to High- Temperature Solar Selective Absorber Materials Review of Mid- to High- Temperature Solar Selective Absorber Materials.
- Kundapur, A., Sudhir, C.V., 2009. Proposal for New World Standard. *J. Eng. Sci. Technol.* 4, 272–281.
- Lamnatou, C., Chemisana, D., 2017. Concentrating solar systems: Life Cycle Assessment (LCA) and environmental issues. *Renew. Sustain. Energy Rev.* 78, 916–932. <https://doi.org/10.1016/j.rser.2017.04.065>.
- Liang, C.J., Liao, J.D., Li, A.J., Chen, C., Lin, H.Y., Wang, X.J., Xu, Y.H., 2014. Relationship between wettabilities and chemical compositions of candle soots. *Fuel* 128, 422–427. <https://doi.org/10.1016/j.fuel.2014.03.039>.
- Liang, C.Y., Krimm, S., 1958. Infrared spectra of high polymers. VI. Polystyrene. *J. Polym. Sci.* 27, 241–254. <https://doi.org/10.1002/pol.1958.1202711520>.

- López-Herrera, M., Fernández, A.B., Martínez, N., Gallas, M., 2017. Effect of the optical properties of the coating of a concentrated solar power central receiver on its thermal efficiency. *Sol. Energy Mater. Sol. Cells* 159, 66–72. <https://doi.org/10.1016/j.solmat.2016.08.031>.
- López-Sosa, L.B., González-Avilés, M., Hernández-Ramírez, M., Medina-Flores, A., Santos-Ramos, I., Zárate-Medina, J., 2019a. Electron microscopy characterization of forest biomass soot as solar energy absorption material. *Microsc. Microanal.* 25, 2234–2235. <https://doi.org/10.1017/s1431927619011905>.
- López-Sosa, Luis Bernardo, Núñez-González, J., Beltrán, A., Morales-Máximo, M., Morales-Sánchez, M., Serrano-Medrano, M., García, C.A., 2019b. A new methodology for the development of appropriate technology: a case study for the development of a wood solar dryer. *Sustain.* 11. <https://doi.org/10.3390/su11205620>.
- López-Sosa, L.B., Zárate-Medina, J., Hernández-Ramírez, L.M., Servín-Campuzano, H., González-Avilés, M., 2018. Development a low-cost solar absorber coating based on soot of biomass-forest: Thermal characterization and application in a solar cooking system. *Rev. Mex. Ing. Quim.* Vol 17, No. 2. Available in <http://www.rmiq.org/ojs311/index.php/rmiq/article/view/76/52>.
- Manzano-Agugliaro, F., Alcalde, A., Montoya, F.G., Zapata-Sierra, A., Gil, C., 2013. Scientific production of renewable energies worldwide: An overview. *Renew. Sustain. Energy Rev.* 18, 134–143. <https://doi.org/10.1016/j.rser.2012.10.020>.
- Martins, J.V., Artaxo, P., Lioussé, C., Reid, J.S., Hobbs, P.V., Kaufman, Y.J., 1998. Effects of black carbon content, particle size, and mixing on light absorption by aerosols from biomass burning in Brazil. *J. Geophys. Res.: Atmos.* 103(D24), 32041–32050. <https://doi.org/10.1029/98JD02593>.
- Masera, O.R., Díaz, R., Berrueta, V., 2005. From cookstoves to cooking systems: the integrated program on sustainable household energy use in Mexico. *Energy Sustain. Dev.* 9, 25–36. [https://doi.org/10.1016/S0973-0826\(08\)60480-9](https://doi.org/10.1016/S0973-0826(08)60480-9).
- Mittal, M., Niles, R.K., Furst, E.M., 2010. Flow-directed assembly of nanostructured thin films from suspensions of anisotropic titania particles. *Nanoscale* 2, 2237–2243. <https://doi.org/10.1039/c0nr00275e>.
- Nannapaneni, R., Chalova, V.I., Crandall, P.G., Ricke, S.C., Johnson, M.G., O'Bryan, C.A., 2009. Campylobacter and Arcobacter species sensitivity to commercial orange oil fractions. *Int. J. Food Microbiol.* 129, 43–49. <https://doi.org/10.1016/j.ijfoodmicro.2008.11.008>.
- Parker, B.F., 1980. Testing and Reporting Solar Collector Performance. Pap. - Am. Soc. Agric. Eng.
- Partal Ureña, F., Moreno, J.R.A., López González, J.J., 2009. Conformational study of (R)-(+)-limonene in the liquid phase using vibrational spectroscopy (IR, Raman, and VCD) and DFT calculations. *Tetrahedron Asymmetry* 20, 89–97. <https://doi.org/10.1016/j.tetasy.2009.01.024>.
- Pino, J.A., Sánchez, M., 2000. Chemical composition of grapefruit oil concentrates. *J. Essent. Oil Res.* 12, 167–169. <https://doi.org/10.1080/10412905.2000.9699489>.
- Prasad, M.S., Mallikarjun, B., Ramakrishna, M., Joarder, J., Sobha, B., Sakthivel, S., 2018. Zirconia nanoparticles embedded spinel selective absorber coating for high performance in open atmospheric condition. *Sol. Energy Mater. Sol. Cells* 174, 423–432. <https://doi.org/10.1016/j.solmat.2017.09.032>.
- Rebollo-Sandoval, H., 2017. Universidad Michoacana de San Nicolás de Hidalgo. Determinación de Comportamiento fototérmico de un recubrimiento hecho a base de hollín. Thesis. Universidad Michoacana de San Nicolás de Hidalgo. Available in: [http://bibliotecavirtual.dgb.umich.mx:8083/xmlui/handle/DGB\\_UMICH/1533](http://bibliotecavirtual.dgb.umich.mx:8083/xmlui/handle/DGB_UMICH/1533).
- Rivera, D.L., Montoya, P.R., Zapata, M.A.T., Ordóñez, K.V., Castrillón, L.J.R., Salazar, Y.V., Carmona, M.E.R., 2014. Tratamiento de residuos de poliestireno expandido utilizando solventes verdes. *Revista Investigaciones Aplicadas* 8 (1), 1–9.
- Roden, C.A., Bond, T.C., Conway, S., Osorto Pinel, A.B., 2006. Emission factors and real-time optical properties of particles emitted from traditional wood burning cookstoves. *Environ. Sci. Technol.* 40, 6750–6757. <https://doi.org/10.1021/es052080i>.
- Sánchez-Cruces, E., Barrera-Calva, E., Lavanderos, K., González, F., 2014. Life cycle analysis (LCA) of solar selective thin films by electrodeposition and by sol-gel techniques. *Energy Procedia* 57, 2812–2818. <https://doi.org/10.1016/j.egypro.2014.10.314>.
- Schulz, H., Baranska, M., 2007. Identification and quantification of valuable plant substances by IR and Raman spectroscopy. *Vib. Spectrosc.* 43, 13–25. <https://doi.org/10.1016/j.vibspec.2006.06.001>.
- Schulz, H., Schrader, B., Quilitzsch, R., Steuer, B., 2002. Quantitative analysis of various citrus oils by ATR/FT-IR and NIR-FT Raman spectroscopy. *Appl. Spectrosc.* 56, 117–124. <https://doi.org/10.1366/0003702021954296>.
- Seidler-Lozykowska, K., Baranska, M., Baranski, R., Krol, D., 2010. Raman analysis of caraway (*Carum carvi* L.) single fruits. Evaluation of essential oil content and its composition. *J. Agric. Food Chem.* 58, 5271–5275. <https://doi.org/10.1021/jf100298z>.
- Servín, H., Peña, M., González, H.S., 2016. Thermal and optical analysis of selective absorber coatings based on soot for applications in solar cookers. *J. Phys. Conf. Ser.* 755. <https://doi.org/10.1088/1742-6596/755/1/011001>.
- Singh, S., Bairagi, P.K., Verma, N., 2018. Candle soot-derived carbon nanoparticles: an inexpensive and efficient electrode for microbial fuel cells. *Electrochim. Acta* 264, 119–127. <https://doi.org/10.1016/j.electacta.2018.01.110>.
- Singh, S., Singh, D., Singh, S.P., Pandey, A.K., 2019. Candle soot derived carbon nanoparticles: assessment of physico-chemical properties, cytotoxicity and genotoxicity. *Chemosphere* 214, 130–135. <https://doi.org/10.1016/j.chemosphere.2018.09.112>.
- Sosa, L.B.L., Avilés, M.G., Pérez, D.G., Gutiérrez, Y.S., 2014. Rural Solar Cookers, an alternative to reduce the timber resource extraction through the use of renewable energy sources: Technology transfer and monitoring project. *Energy Procedia* 57, 1593–1602. <https://doi.org/10.1016/j.egypro.2014.10.151>.
- Soto, L., Ojeda de Rodríguez, G., Rojas, L., Sulbarán, B., Peña, J., Berradre, M., Fernández, V., 2013. Caracterización química del aceite esencial de toronja (*Citrus paradisi* L.). *Rev. la Fac. Agron.* 30, 266–283.
- Su, Z., Zhou, W., Zhang, Y., 2011. New insight into the soot nanoparticles in a candle flame. *Chem. Commun.* 47, 4700–4702. <https://doi.org/10.1039/c0cc05785a>.
- Suryanarayana, C., 2004. Mechanical alloying and milling. *Mech. Alloy. Milling* 1–472. <https://doi.org/10.4150/kpmi.2006.13.5.371>.
- Susi, T., Pichler, T., Ayala, P., 2015. X-ray photoelectron spectroscopy of graphitic carbon nanomaterials doped with heteroatoms. *Beilstein J. Nanotechnol.* 6, 177–192. <https://doi.org/10.3762/bjnano.6.17>.
- Wamae, W., Suriwong, T., Threrujirapong, T., 2018. Influence of tin content on spectral selectivity and thermal conductivity of Sn–Al<sub>2</sub>O<sub>3</sub> solar selective absorber. *Mater. Renew. Sustain. Energy* 7, 1–8. <https://doi.org/10.1007/s40243-017-0109-1>.
- Wan, D., Komvopoulos, K., 2007. Tetrahedral and trigonal carbon atom hybridization in thin amorphous carbon films synthesized by radio-frequency sputtering. *J. Phys. Chem. C* 111, 9891–9896. <https://doi.org/10.1021/jp071750z>.
- Xie, Q., Zhou, S., Wu, S., Zhang, Y., Zhao, P., 2017. Supercapacitive behavior of laminar-structured carbon cloth with alternating graphene and hybrid nanofibers: a synergistic effect of graphene-coating and post-oxidation. *Appl. Surf. Sci.* 407, 36–43. <https://doi.org/10.1016/j.apsusc.2017.02.172>.
- Xue, G., Liu, K., Chen, Q., Yang, P., Li, J., Ding, T., Duan, J., Qi, B., Zhou, J., 2017. Robust and low-cost flame-treated wood for high-performance solar steam generation. *ACS Appl. Mater. Interfaces* 9, 15052–15057. <https://doi.org/10.1021/acsami.7b01992>.
- Zhang, Y.Y., Chen, S., Xiang, H., Gong, X.G., 2016. Hybrid crystalline sp<sup>2</sup>[Formula presented]3 carbon as a high-efficiency solar cell absorber. *Carbon N. Y.* 109, 246–252. <https://doi.org/10.1016/j.carbon.2016.08.015>.